

# A comparison between joint level torque sensing and proximal F/T sensor torque estimation: implementation on the iCub

M. Randazzo, M. Fumagalli, F. Nori, L.Natale, G. Metta, G. Sandini

**Abstract**— When a robot is required to safely interact with a physical environment, two approaches are typically reported in literature: using a force/torque sensor to regulate the interaction forces at the end effector, or integrating sensors in each robot joint to regulate their torques. In this paper we want to discuss the benefits and the disadvantages of the two approaches, showing a direct comparison between the information which can be obtained from the two categories of sensors. Results obtained on the new iCub arm, which integrates torque sensing capabilities at joint level will be presented and discussed.

## I. INTRODUCTION

Recent trends and future perspectives are defining new guidelines of robotic research. Autonomous robots, and more in particular humanoid robots, should be capable of coexisting with humans in dynamical environments, thus properly controlling their reaction forces when interacting with objects that belong to their operative space or when unpredicted events occur, such as accidental impacts with humans or with objects they have to manipulate [1].

In order to obtain compliant actuation, *passive* elements (i.e. mechanical springs) are often introduced in robotic mechanisms in order to decouple the inertia of the motor (typically high) from the inertia of the controlled joint [2]. This solution has the advantage of being intrinsically safe; however the mechanical bandwidth of the system is determined by the fixed stiffness of the passive spring.

A completely different approach is represented by systems in which the compliance is not obtained by the introduction of mechanical elements but by virtue of a controller, which *actively* regulates the interaction forces in order to obtain a virtual compliance at the end-effector. In such a system the robot is thus equipped with joint torque sensors or force sensors (the latter typically placed at the end-effector), which provide the feedback information needed by the closed loop control system [3][4]. By exploiting the information obtained through these sensors, the robot can not only react to external interaction forces, but also create a proper haptic representation of a surrounding unknown environment.

This work was supported in part by the European Projects: VIATORS (FP7-ICT-2007-3), CHRIS (FP7-IST-215805) and ITALK (ICT-214668).

All the authors are with the Robotics, Brain and Cognitive Sciences Department, Italian Institute of Technology, Genoa, Italy.

G. Metta and G. Sandini are also with the Department of Communications, Computer and System Sciences, Faculty of Engineering, University of Genoa, Italy.

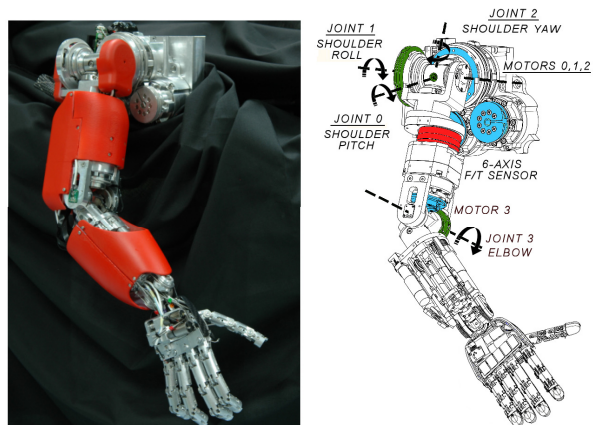


Fig. 1: *Left*: The new iCub arm with integrated joint torque sensors. *Right*: a CAD view of the arm showing its main DoFs, the location of the motors (blue), the six-axis force/torque sensor (red) and the integrated joint torque sensors (green). The coupled joints/motors are underlined.

In this paper we address the issue of improving the perception of the robot-environment interaction exploiting both joint torque sensors and six-axis F/T sensors. On this argument, previous work can be found for industrial manipulators in [5][6]. In this work, experiments will be conducted on a prototype of the iCub humanoid platform equipped with both type of sensors plus an artificial skin which allows determining the external point of contact. A comparison between the information which can be retrieved from the two categories of sensors will be presented. It will be shown that using only localized joint torque sensors might not allow a full perceptual representation of the interaction scenario, since singular configurations exist where some interaction forces cannot be fully measured (e.g. pure forces working on a direction which is parallel to the joint torque sensor axis are hidden). On the other hand, although six-axis force/torque sensors give a more complete representation of the interaction, the estimation of joint torques requires additional calculations and results may be affected by computation delays and model errors. It will be also discussed the importance of the location of the force/torque sensor along the robot kinematic chain. In fact, while this kind of sensor is traditionally mounted at the end-effector to directly sense the interaction forces, such a location does not allow retrieving neither the information about the manipulator dynamics, nor about the potential interaction occurring on any link of the arm. The solution addressed in the design of the iCub robot, instead, makes use of a force/torque sensor embedded in the arm placed

distally with respect to the end-effector (i.e. the hand). In such a configuration, both dynamical wrenches (i.e. the forces and moments that are due to the dynamics of the structure) and the external interaction forces can be measured. Finally it will be shown how is possible to calibrate the joint-level torque sensors by exploiting the torque estimation obtained through the six-axis force/torque sensor.

## II. THE EXPERIMENTAL PLATFORM

A comprehensive description of the structure of the *new iCub arm*, which features several mechanical improvements such as the integration of torque sensors directly on its joints, is reported in [7] and here briefly summarized.

The iCub arm is a 7DoF manipulator (Figure 1). The first 4DoF correspond to the shoulder, which is functionally equivalent to a 3DoF spherical joint, plus the elbow (1DoF). For all these joints a direct sensing of the joint torque is available through strain gauges which have been conveniently mounted on the structure. Additionally, the arm is equipped with a custom-made six-axis force/torque sensor [8], mounted between the shoulder and the elbow joint, and an array of capacitive tactile sensors [9][10], which can be used to respectively estimate the arm joint torques and the localize the external contacts (Figure 2).

The remaining 3DoF of the iCub arm constitute the wrist. For these joints, however, an integrated joint torque sensor is not yet available, basically because the intrinsic elasticity of this part and the space constraints (the wrist actuation is obtained through a compact differential tendon-driven mechanism), requires a different way of sensing the torques. As to this concern, we performed preliminary studies for different applications, with strain gauges mounted on cantilever structures [11] or directly on the tendons [12], while a solution for the iCub wrist is still under investigation.

For these reasons, in this paper we will focus on only the first four joints (shoulder+elbow) of the iCub arm, since for the wrist joints a direct comparison between sensed and computed torques is not possible at the present time.

### A. The iCub arm coupling mechanism

The iCub shoulder is a complex differential mechanism constituted by three brushless motors coupled by a cable transmission. The first motor actuates directly the joint 0 (shoulder pitch), whereas the other two motors actuate joints 1 and 2 through a set of coaxial pulleys of different diameter (Figure 1). The ratio of the diameters of these pulleys defines a transmission reduction  $r$ . The resulting relationship between the motor angular velocities  $\dot{\theta}_m$  and the joint velocities  $\dot{\theta}_j$  takes thus the following linear form:

$$\dot{\theta}_m = T \dot{\theta}_j \quad T = \begin{bmatrix} 1 & 0 & 0 \\ -r & r & 0 \\ -r & r & r \end{bmatrix} \quad (1)$$

From the previous equation (1), the relationship between

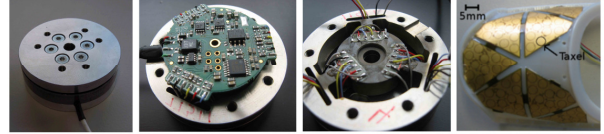


Fig. 2: *from left to right*: the custom six-axis F/T sensor mounted on the iCub arm; the internal electronic board that provides signal conditioning and acquisition; the strain gauges mounted on the back of electronic board; the iCub forearm plastic cover, with embedded tactile sensors.

the motor torques  $\tau_m$  and the joint torques  $\tau_j$  can be derived. Let's consider the power conservation equation:

$$\delta W_m = \delta W_j \rightarrow \tau_m^T \dot{\theta}_m = \tau_j^T \dot{\theta}_j \quad (2)$$

By substituting (1) in (2) we obtain:

$$\tau_m^T T \dot{\theta}_j = \tau_j^T \dot{\theta}_j \rightarrow T^T \tau_m = \tau_j \quad (3)$$

which can be written in order to express the joint torques  $\tau_j$  as a function of the motor torques  $\tau_m$ :

$$\tau_m = T^{-T} \tau_j \quad T^{-T} = \begin{bmatrix} 1 & 1 & 0 \\ 0 & 1/r & -1/r \\ 0 & 0 & 1/r \end{bmatrix} \quad (4)$$

Remarkably, we can notice from the first line of the matrix  $T^{-T}$  that the torque of motor 0 can be expressed as a function of the torques of joints 0 and 1. Since in our system the torque sensor of the joint 0 is located right on the motor shaft, the knowledge of this relationship is required to decouple the measurements of the joint sensor 0 from those of the joint sensor 1. This concept is further clarified in the next subsection.

### B. Joint torque sensing on iCub arm

As previously mentioned, the new iCub arm integrates torques sensing capabilities directly on its joints. This is obtained through the placement of semiconductor strain gauges (SSGs) on ad-hoc redesigned mechanical parts. More in particular, the location for the four joint torque sensors was chosen to be as follows:

1) *Elbow joint*: this is the simplest case, since the elbow joint takes no part in the coupling mechanism of the shoulder and is controlled by its own independent motor. The torque of this joint is measured by two SSGs mounted on a spoke-structure, which has been conveniently introduced on a modified mechanical part (Figure 3). The two strain gauges are configured as an half Wheatstone bridge (the other half of the bridge is directly mounted on the acquisition board) and the output signal is acquired by a 16-bits ADC converter. The resulting joint torque  $\tau_{elbow}$  can be thus obtained from the raw measurements of the sensor ( $s_j$ ) accordingly to the following formula:

$$\tau_{elbow} = c_1 \cdot (s_1 + o_1) \quad (5)$$

where  $c_j$  represents the calibration coefficient required to convert from arbitrary units (i.e. the 16-bits integers returned by the analog-to-digital converter) to metric measurements (Nm), and  $o_j$  represents the sensor offset

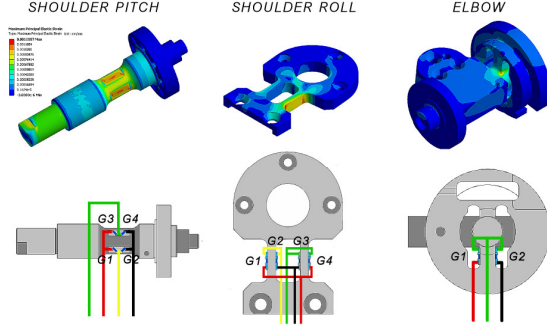


Fig. 3: *Top*: the sensorised mechanical parts. Finite element simulations are performed in order to choose the optimal location of the strain gauges. *Bottom*: each couple of sensors is configured as a half Wheatstone bridge.

which has to be canceled out so that the sensor measurement is zero when no torque is applied to the joint.

2) *Shoulder yaw*: since the rotational axis of this joint is parallel to the z-axis of the six-axis force-torque sensor (see Figure 1) mounted between the shoulder and the elbow, it was chosen not to add additional SSGs on this joint. Instead, the joint torque ( $\tau_{yaw}$ ) can be simply computed by considering the fixed displacement  $d=15mm$  between the two axis, and the quantities  $T_z$  (the torque along the z-axis) and  $F_y$  (the force along the y-axis) measured by the six-axis F/T sensor:

$$\tau_{yaw} = F_y \cdot d + T_z \quad (6)$$

3) *Shoulder roll*: a new part, constituted by two beam-like structures was added to the transmission pulley on the joint side. Two couples of SSGs, each of them constituting its own Wheatstone half bridge, are acquired separately by two independent input channels ( $s_2, s_3$ ) of the acquisition board. The joint torque ( $\tau_{roll}$ ) can be thus computed as:

$$\tau_{roll} = c_2 \cdot (s_2 + o_2) + c_3 \cdot (s_3 + o_3) \quad (7)$$

It must be noticed that in this case two calibration coefficients ( $c_2, c_3$ ) and two sensor offsets ( $o_2, o_3$ ) are employed, in order to take in account the small mismatch in sensitivity due to the manual gluing process of the strain gauges couples. Finally, it must be pointed out that, since the sensorised part is mounted on the joint *after* the coupled transmission of the shoulder, the measurement of the strain gauges are not influenced by the torques applied on the other shoulder joints.

4) *Shoulder Pitch*: as shown in equation (1), this is the only degree of freedom directly controlled by a single motor (i.e. the motor output shaft is rigidly attached to shoulder joint without any cable transmission). We thus chose to directly sensorise a new hollow motor shaft with two couples of SSGs placed at ninety degrees from each other. Each couple of strain gauges is thus configured as a half Wheatstone bridge and the two measurements ( $s_4, s_5$ ) are acquired by two independent input channels, as in the case of the shoulder roll joint. However, in this case the sensor does not only measures the joint torque, but also the

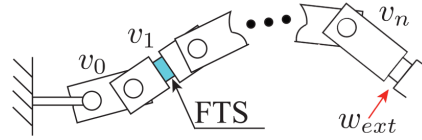


Fig. 4: An illustrative sketch of a robotic serial manipulator. The unknown external wrench  $w_{ext}$  can be computed through the information provided by the six-axis force/torque sensor mounted in the middle of link 1.

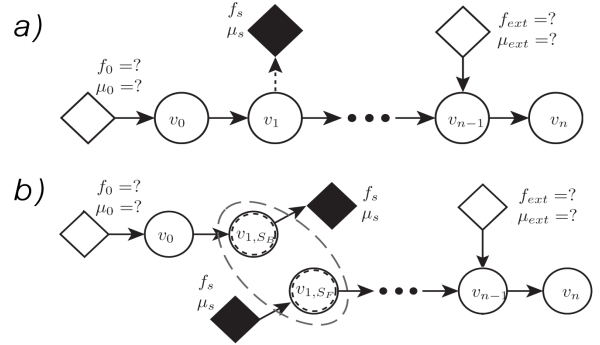


Fig. 5a: representation of the robotic mechanism of Fig. 4, with the enhanced graph formulation. Fig. 5b: force/torque sensors embedded in links allow splitting the chain into two sub-chains.

torsion on the motor shaft induced back by the shoulder roll joint through the cable coupling. In fact, it has been shown in equation (4) that the relationship between motor torques and joint torques can be expressed through a transformation matrix which depends on the topology of the coupling mechanism. Taking in account this relationship, the torque of the shoulder pitch joint can be expressed as:

$$\tau_{pitch} = c_4 \cdot (s_4 + o_4) + c_5 \cdot (s_5 + o_5) - \tau_{roll} \quad (8)$$

Also in this case two calibration coefficients ( $c_4, c_5$ ) and two offsets ( $o_4, o_5$ ) are required to obtain a calibrated measurement. These parameters are determined with the procedure described in section III.

### C. Computed joint torques approach

A model based approach [13] has been developed for the iCub humanoid robot, which exploits a graph formulation to compute the inverse dynamics of the system.

The method makes use of graph theory to introduce in the computation of the dynamics the measurements from the six-axis force/torque sensors and the contact point information retrieved from the iCub artificial skin. Figure 4 shows an illustrative example of a robotic serial mechanism equipped with a force/torque sensor in one of its links. Through this sensor it is possible to measure both the components (forces and moments) of the wrench which are due to the internal dynamics of the robot, but also a single external wrench applied distally with respect to the sensor.

Let us represent the serial mechanism of Figure 4 with an oriented graph formulation, in which each vertex  $v_i$  represents the  $i$ -th link and each outgoing edge represents the reference frame constrained to the  $i$ -th link (Figure 5a).

Let us consider that the unknown wrenches of this robotic mechanism are the externally applied wrench  $\mathbf{w}_{ext}=(f_i, \mu_i)$  and the reaction forces on the base  $\mathbf{w}_0=(f_0, \mu_0)$ , both graphically represented by a white rhombus ( $\diamond$ ). Let us also consider the known quantities  $\mathbf{w}_s=(f_s, \mu_s)$ , graphically indicated by a black rhombus ( $\blacklozenge$ ), which correspond to the wrench measured by the force/torque sensor. In order to compute the unknown wrenches, the presence on one link of a force/torque sensor can be exploited to split the kinematic chain into two sub-chains, each of them having as a boundary the known wrench  $\mathbf{w}_s=(f_s, \mu_s)$  given by the sensor measurements. Figure 5b shows the effect of the splitting of the chain of Figure 5a into two sub-chains. It is remarkable that for each sub-chain there is one single unknown ( $\diamond$ ), which is the quantity that can be computed through the classical Newton-Euler recursion.

The computation of the unknown thus follows the rule of a preordered traversal visit of the graph. First the kinematic variables (velocities/accelerations) are propagated from the base to the end-effector, using the information of an inertial sensor to initialize the computations. Secondly, the known wrenches are propagated from the known nodes ( $\blacklozenge$ ) to the unknown nodes ( $\diamond$ ), assuming that the dynamical parameters (mass, center of gravity, inertia matrix) of the visited nodes (i.e. of the robot links) are known. Remarkably, this operation can be performed only if it exists one unique unknown for each sub-graph. As a consequence, given N force/torques sensors distributed on robotic chain, N+1 sub-graphs are produced and therefore a maximum of N+1 external wrenches can be estimated (one for each sub-graph).

The method graphically represents the flowing of the information of wrenches within a chain. Moreover, it can be noticed that, while the structure of the graph with its link nodes and known nodes ( $\blacklozenge$ ) are fixed a priori, the way the graph is visited changes depending on the position of the external contact (an information that can be retrieved through a network of tactile sensors, such as the iCub artificial skin). In fact, this formulation allows varying dynamically the position of the unknown ( $\diamond$ ), and thus also the numbering scheme for visiting the graph and performing the calculation is dynamically computed.

Finally, it should be noticed that, given the estimation of all the internal wrenches  $\mathbf{w}$  of the structure, the joint torque  $\tau_i$  can also be retrieved projecting the moment  $\mu_i$  along the axis of rotation of the joint placed on the frame  $i$ .

#### D. Torques estimation on the iCub robot

From the architectural point of view, we centralized the computation of the estimated joint torques in a single software module (namely, the *whole body torque observer*<sup>1</sup>)

<sup>1</sup> The module is part of the iDyn package [14], a C++ opensource library developed by the authors for computing forward/inverse

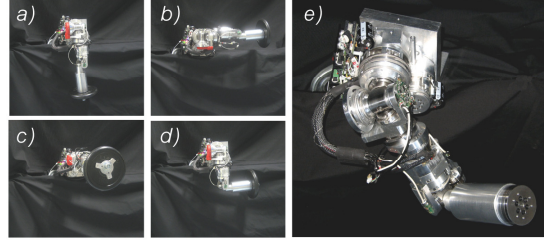


Fig.6: The key configurations assumed by the arm during the calibration procedure: a) rest position b) max torque for the shoulder pitch c) max torque for the shoulder roll d) max torque for the elbow joint e) the shoulder with the additional F/T sensor located on the end effector.

which runs on a standard PC, while the position/force control loops run locally on DSP-based control boards. The kinematic information (e.g. the joint angular positions, velocities etc.) is broadcasted by the DSPs on local CAN buses, collected by a PC104 board and transmitted to the torque observer module through a Gigabit Ethernet connection. After the computation, the estimated joint torques are retransmitted back to the control boards. The whole process takes about ten milliseconds. Remarkably, we decided to use the same protocol to identify the torque measurement transmitted on the CAN bus line by the real joint torque sensors and by the observer module. This solution provides the following advantages:

1) In the case of a joint sensor failure, the control board can seamless switch from the real joint sensor measurements to the estimated ones (a sort of recovery strategy that allows not compromising the safety of the robot interaction with the environment).

2) The computed joint torques estimations can be used to calibrate the joint torques sensors directly on the robot. In fact, due to the complexity of the shoulder mechanism, it is not possible to individually calibrate the joint torque sensors before the complete assembly of the arm. The procedure for the calibration of the joint torque sensors is described in section III.

### III. CALIBRATION OF THE INTEGRATED JOINT TORQUE SENSORS

As mentioned in section II-B, the calibration of the integrated joint torque sensors employs a linear model, consisting in a certain number of scaling coefficients and offsets, justified by the extremely linear response of the SSGs in the region of the admissible strain ( $\pm 1000\mu\epsilon$ ).

In order to determine the calibration parameters, two different procedures can be followed:

1) A known weight is attached to the robotic arm. The arm joints are moved in known kinematic configurations which simplify the computation of applied torques. The

kinematics and dynamics of serial-link chains, with the approach described in section II-C.

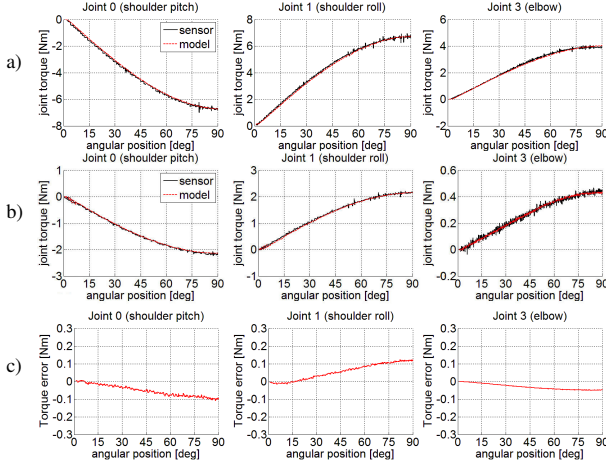


Fig. 7a: The measured and predicted torques during the calibration of the three joint torque sensors. Fig. 7b: The measured and predicted torques due to the gravity force acting on the arm links. Fig. 7c: The differences between the measurements of the sensors calibrated with only the gravity force and with external weights.

applied known torques are then matched against the raw sensory data and the calibration parameters are computed through a linear least-squares regression.

2) We can take advantage of the six-axis F/T sensor to estimate the joint torques with the method described in section II-C. The estimated torques are then matched against the raw sensory data and the calibration parameters are computed through a linear least-squares regression.

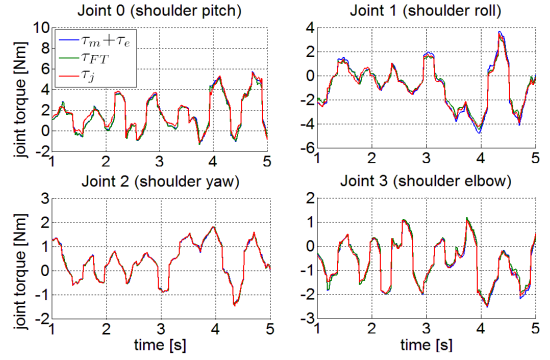
#### A. Sensors calibration with known weights

In order to calibrate the joint torque sensors, the forearm and the hand have been removed from the robotic platform and substituted with a cylinder of equivalent mass, to which external weights can be attached. The arm is subsequently moved to known kinematic configurations in which the developed joint torques are maximum (Figure 6a-6d).

The results of the sensors calibration are reported in Figure 7a. The corresponding errors are comparable with the intrinsic noise level of the controlled system (about 0.02Nm), thus demonstrating a very good linearity of the sensors in the calibration range.

#### B. Sensors calibration through estimated joint torques

As previously mentioned, an alternative calibration method consists in taking advantage of the proximal six-axis F/T sensor in order to estimate the joint torques, and use this estimation to calibrate the joint sensors. This solution has the advantage that can be employed to calibrate the torque sensors anytime (i.e. even when the robot hand is fully assembled) and does not require the application of external weights, which are difficult to attach to the robotic wrist. With the assumption that no external forces are acting on the robot, the sensors measurements are thus matched against the estimated torques due to the gravity force acting



	Joint 0	Joint 1	Joint 2	Joint 3
$E(\tau_j - \tau_{\hat{j}})$	0.127 Nm	-0.049 Nm	-0.002 Nm	-0.032 Nm
$\sigma(\tau_j - \tau_{\hat{j}})$	0.186 Nm	0.131 Nm	0.013 Nm	0.042 Nm
$E(\tau_j - (\tau_m + \tau_e))$	0.075 Nm	-0.098 Nm	-0.006 Nm	0.006 Nm
$\sigma(\tau_j - (\tau_m + \tau_e))$	0.191 Nm	0.173 Nm	0.020 Nm	0.032 Nm

Fig. 8: A comparison between the measured joint torques ( $\tau_j$ ), the ones computed using the F/T sensor embedded in the arm ( $\tau_{FT}$ ) and the ones estimated through the additional sensor located at the end effector ( $\tau_m + \tau_e$ ). The table reports the mean and the standard deviation of the prediction errors for both the quantities  $\tau_j - \tau_{FT}$  and  $\tau_j - (\tau_m + \tau_e)$ .

on the robot links in static configurations (in order to measure joint torques from FT measurement, we in fact need to perform time consuming computation and therefore only in static conditions our measurement can be considered not affected by delays).

Results obtained with this calibration procedure are shown in Figure 7b. It can be noticed that since no weights are applied, the calibration range (i.e. the maximum developed torques) is substantially smaller respect to the previous case. Moreover, since we are relying on a sensor which itself may be affected by small calibration errors, we have to compare the obtained results with the ones obtained with the procedure described in section III-A. Such a comparison is reported in Figure 7c. The plots show a substantial agreement between the two calibration procedures, with a maximum error of 0.1 Nm.

## IV. COMPARISON BETWEEN THE APPROACHES

In this section a set of different experiments is presented to compare the estimations computed through the method described in section II-C with the measurements obtained by the calibrated joint torque sensors.

Hereafter we will indicate the estimated wrenches and joint torques with the subscript **ft**, to emphasize that fact that we are referring to *estimations computed from the six-axis force/torque sensor* located in the robot arm, while the measurements obtained from the joint sensors will have the subscript **j** (*joint torque sensor measurements*). Moreover, we will use the subscript **e** to indicate the *external* wrenches applied at the end effector and the corresponding joint torques (computed by projecting the external wrenches by the transposed Jacobian, i.e.:  $\tau_e = J^T w_e$ ). Finally, we will indicate with the subscript **m** the *model torques* predicted

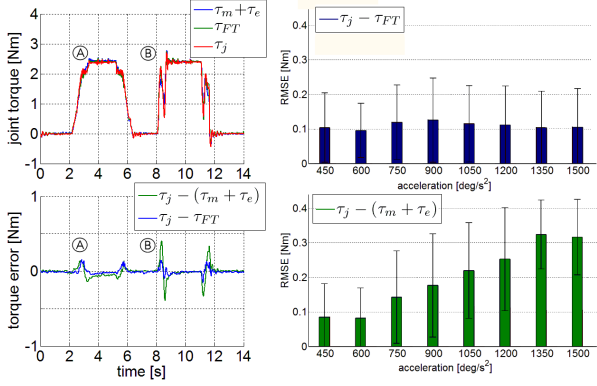


Fig. 9: *Left*: Measured and predicted joint torques during: A) a trajectory performed at 90deg/s; B) the same trajectory performed at 180deg/s. *Right*: the prediction errors.

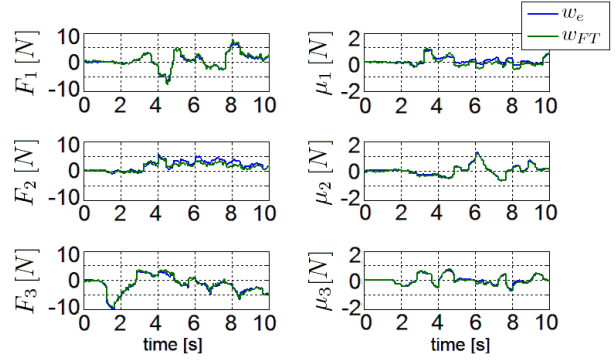
by the arm dynamical model which does not take into account the externally applied forces.

#### A. Model validation in a static configuration

For this experiment we placed an additional six-axis force/torque sensor on the extremity of the robotic arm (Figure 6e) in order to accurately measure the external wrenches  $w_e$ . The arm is therefore controlled in position so that the resulting joint torques ( $\tau_j$ ) are only due to the robot reaction to the manually applied external wrenches ( $\tau_e = J^T w_e$ ) and the gravity acting on its links ( $\tau_m$ ). Figure 8 shows a comparison between the real measurements  $\tau_j$  and the quantities  $\tau_m + \tau_e$  and  $\tau_{ft}$ , which should be ideally identical in the case of perfect estimations. Remarkably, a good agreement is shown between the three quantities with a resulting prediction error smaller than 0.2Nm for all the four joints.

#### B. Estimation of joint torques due to robot dynamics

In order to validate our estimations in the dynamic case we commanded the robot to perform fast repetitive movements with a weight attached to its end effector. In particular, results presented in Figure 9 refer to a movement of the elbow joint only, with an attached weight of 1Kg, performed at two different velocities: 90 and 180deg/s. Results show a generally good correspondence between the measurements ( $\tau_j$ ) and the predictions ( $\tau_{ft}$  and  $\tau_m + \tau_e$ ), however some errors can be noticed which can be explained as follows. Both the quantities  $\tau_{ft}$  and  $\tau_m + \tau_e$  are estimations computed from F/T sensors using the framework introduced in section II-C. However for the elbow movement we are considering, it must be noticed that  $\tau_{ft}$  uses only static information (i.e. not affected by velocities/accelerations) while  $\tau_m + \tau_e$  uses also dynamic information. Since these last quantities are not directly measured, but estimated through computations and filtering, they are affected by a noise which increases with the acceleration, as shown in Figure 9. As an additional remark, it is worth noting that these



	$F_1$ (N)	$F_2$ (N)	$F_3$ (N)	$\mu_1$ (Nm)	$\mu_2$ (Nm)	$\mu_3$ (Nm)
$E(w_e - w_{FT})$	0.181	-0.465	-0.154	-0.079	-0.024	-0.024
$\sigma(w_e - w_{FT})$	0.384	0.426	0.469	0.149	0.048	0.059

Fig. 10: A comparison between the measured and the predicted external wrenches. First row, average error; second row, standard deviation.

dynamic errors increase with the kinematic distance between the F/T sensor and the joint of which we are estimating the torque (i.e. the higher is the number of the joints which take part in the computation, the higher is noise which affects the estimation of speeds and accelerations).

#### C. Representation of the external wrenches

The approach described in section II-C allows retrieving not only an estimation of the joint torques as just shown, but also a single externally applied wrench. If we consider the same experiment described in IV-A, we can compare the measurements of the externally applied wrenches  $w_e$  (i.e. the wrenches measured with the external force/torque sensor located at the end effector), with the estimation  $w_{ft}$  computed from the sensor mounted on the iCub shoulder. Figure 10 shows the result of this comparison. Remarkably, it is not possible to compute an estimation of the externally applied wrenches  $w_e \in R^6$  using the only measurements of joint torques  $\tau_j \in R^4$ . On the contrary a good correspondence is shown between the measurements  $w_e$  and the estimations  $w_{ft}$ , with a maximum prediction error of 0.48N for the forces and 0.16Nm for the moments.

## V. CONCLUSION

In this paper it was shown a comparison between the information which can be directly retrieved from integrated joint-level torque sensors and the estimation computed through a six-axis torque force sensor mounted distally respect to end-effector. A model based approach has been presented, which allows retrieving, under suitable assumptions, joint torques and external wrenches applied on a single known location. Remarkably, it has been shown that two conditions have to be fulfilled in order to perform the propagation of the force information along the kinematic chain:

- 1) The computation of the arm dynamics in the presence

of an external force requires the exact knowledge of its application point. In order to perform the calculation, this point can be either considered fixed a priori (for example assuming that all the interactions with the environment may occur at the end-effector, i.e. the iCub hand) or can dynamically change as a function of the estimated point of contact. In this latter case, a set of distributed tactile sensors, such as the iCub artificial skin [9][10], has to be employed in order to obtain the location of the contact point and to dynamically define the topology of the graph used for the computation of joint torques. It must be noticed, on the contrary, that joint-level torque sensors provide direct measurements of the torques, and in this case the knowledge of the external forces application point is obviously not required.

2) Inertial measurements, which on the iCub platform are provided by an inertial sensor located in the robot head, are required to initialize the kinematics computations by propagating the measured linear/angular velocities and accelerations to all the robot links. In absence of such information, an a priori assumption (i.e. the orientation of the gravity force acting on the robot links) has to be employed. Also in this case, a robot equipped with joint torque sensors can directly obtain torque measurements even in the absence of an inertial sensor.

One final consideration regards the hardware/software complexity of the two approaches. Of course it can be noticed that estimating the joint torques through a model-based approach with the employment of a single additional force/torque sensor placed in the middle of a kinematic chain is for certain aspects convenient. In a sense, this approach allows adding force sensing capabilities to preexisting robots with minimal mechanical modifications. On the contrary, the integration of joint-level torque sensors in a non-modular system like the iCub arm implies a remarkable increase of the *hardware complexity* in terms of additional wiring and mechanical design. Finite element simulations must be in fact performed to select the best sensor placement, which can be different for each joint.

On the other hand it must be noticed that a model-based approach increases the *software complexity*. On the iCub arm real torque measurements are broadcasted by the torque sensors on the CAN bus line every millisecond. With the estimated torques approach, instead, a new measurement is computed every ten milliseconds. This fixed delay obviously implies that the controller will react to external forces with a certain latency, which may be acceptable or not, depending on the application and the level of safety which has to be guaranteed [15].

With respect to this last point, it must be noticed that one of the current research trends in the field of physical human-robot interaction is the development of novel, intrinsically compliant actuation concepts. Variable

impedance actuators, for example, exploit particular mechanical designs [16][17] to actively regulate the stiffness of integrated elastic elements, thus combining the benefits of the traditional passive and active paradigms. Since in these systems it is mandatory to control both the joint torque and joint stiffness with the fastest possible control loop, the integration of torque measurement systems directly on the joint/actuator seems to be a mandatory design constraint.

## REFERENCES

- [1] S. Haddadin, A. Albu-Schaffer and G. Hirzinger, "The role of the robot mass and velocity in physical human-robot interaction", In Proc. IEEE Int. Conf. on Robotics and Automation, 2008.
- [2] G. Pratt, and M. Williamson, "Series elastic actuators", In IEEE/RSJ Int. Conf. on Intelligent Robots and Systems, 1995.
- [3] J. Luh, W. Fisher, and R. Paul, "Joint torque control by a direct feedback for industrial robots," IEEE Trans. on Automatic Control, vol. 28, no. 2, pp. 153-161, 1983.
- [4] F. Aghili, M. Buehler, and J. Hollerbach, "A joint torque sensor for robots," in ASME Int. Mechanical Engineering Congress, 1997.
- [5] Helmick, David, Okon, Avi DiCicco, Matt. A comparison of force sensing techniques for planetary manipulation. 2006 IEEE Aerospace Conference, Big Sky, MT, March 2006.
- [6] J. Gamez, A. Robertsson, J. Gomez Ortega, and R. Johansson, Sensor fusion for compliant robot motion control. IEEE Trans. on Robotics, 24(2): pp.430-441, 2008.
- [7] A. Parmiggiani, M. Randazzo, L. Natale, G. Metta, and G. Sandini, "Joint torque sensing for the upper-body of the iCub humanoid robot," in Int. Conf. on Humanoid Robots, Paris, France, 2009.
- [8] M. Fumagalli, M. Randazzo, F. Nori, L. Natale, G. Metta, and G. Sandini, "Exploiting proximal F/T measurements for the iCub active compliance," in Int. Conf. on Intelligent Robots and Systems, 2010.
- [9] G. Cannata, M. Maggiali, G. Metta, and G. Sandini, "An embedded artificial skin for humanoid robots," in IEEE Int. Conf. on Multisensor Fusion and Integration, pp.434-438, Seoul, Korea, 2008.
- [10] A. Del Prete, S. Denei, L. Natale, F. Mastrogiovanni, F. Nori, G. Cannata, G. Metta, "Skin Spatial Calibration Using Force/Torque Measurements", in Int. Conf. on Intelligent Robots and Systems, San Francisco, CA, USA, 2011.
- [11] M. Fumagalli, L. Jamone, G. Metta, L. Natale, F. Nori, A. Parmiggiani, M. Randazzo and G. Sandini, "A Force Sensor for the Control of a Human-like Tendon Driven Neck," 9th IEEE-RAS Int. Conf. on Humanoid Robots, pp.478-485, Paris, France, 2009.
- [12] M. Randazzo, M. Fumagalli, F. Nori, G. Metta and G. Sandini, "Force control of a tendon driven joint actuated by dielectric elastomers", Int. Conf. on New Actuators, Bremen, Germany, 2010.
- [13] M. Fumagalli, S. Ivaldi, M. Randazzo, F. Nori, G. Metta, G. Sandini, "Force feedback exploiting tactile and proximal force/torque sensing: theory and implementation on the humanoid robot iCub", submitted to Autonomous Robots, 2011
- [14] S. Ivaldi, M. Fumagalli, and U. Pattacini, "iDyn documentation" [http://eris.liralab.it/iCub/main/dox/html/group\\_iDyn.html](http://eris.liralab.it/iCub/main/dox/html/group_iDyn.html).
- [15] S. Haddadin, A. Albu-Schaffer and G. Hirzinger, "Safety evaluation of physical human-robot interaction via crash-testing", in Robotics: Science and System Conference, pp. 217-224, Atlanta, USA, 2007.
- [16] R. Schiavi, G. Grioli, S. Sen, and A. Bicchi. VSA-II: A Novel Prototype of Variable Stiffness Actuator for Safe and Performing Robots Interacting with Humans. In Proc. IEEE Int. Conf. on Robotics and Automation, pp. 2171-2176, Pasadena, USA, 2008.
- [17] A. Jafari, N. Tsagarakis, B. Vanderborght, D.G. Caldwell, A Novel Actuator with Adjustable Stiffness(AwAS), IEEE/RSJ Int. Conf. on Intelligent Robots and Systems, pp. 4201-4206, Taipei, Taiwan, 2010.